

# Oxidative ATP synthesis in skeletal muscle is controlled by substrate feedback

Fan Wu, Jeroen A. L. Jeneson and Daniel A. Beard

*Am J Physiol Cell Physiol* 292:115-124, 2007. First published Jul 12, 2006;  
doi:10.1152/ajpcell.00237.2006

## You might find this additional information useful...

---

This article cites 26 articles, 17 of which you can access free at:

<http://ajpcell.physiology.org/cgi/content/full/292/1/C115#BIBL>

This article has been cited by 10 other HighWire hosted articles, the first 5 are:

### **Magnitude and control of mitochondrial sensitivity to ADP**

J. A. L. Jeneson, J. P. J. Schmitz, N. M. A. van den Broek, N. A. W. van Riel, P. A. J. Hilbers, K. Nicolay and J. J. Prompers

*Am J Physiol Endocrinol Metab*, September 1, 2009; 297 (3): E774-E784.

[Abstract] [Full Text] [PDF]

### **Interpreting the phosphocreatine time constant in aerobically exercising skeletal muscle**

G. Kemp

*J Appl Physiol*, January 1, 2009; 106 (1): 350-350.

[Full Text] [PDF]

### **Role of NADH/NAD<sup>+</sup> transport activity and glycogen store on skeletal muscle energy metabolism during exercise: in silico studies**

Y. Li, R. K. Dash, J. Kim, G. M. Saidel and M. E. Cabrera

*Am J Physiol Cell Physiol*, January 1, 2009; 296 (1): C25-C46.

[Abstract] [Full Text] [PDF]

### **Physiological implications of linear kinetics of mitochondrial respiration in vitro**

G. Kemp

*Am J Physiol Cell Physiol*, September 1, 2008; 295 (3): C844-C846.

[Full Text] [PDF]

### **Phosphate metabolite concentrations and ATP hydrolysis potential in normal and ischaemic hearts**

F. Wu, E. Y. Zhang, J. Zhang, R. J. Bache and D. A. Beard

*J. Physiol.*, September 1, 2008; 586 (17): 4193-4208.

[Abstract] [Full Text] [PDF]

Updated information and services including high-resolution figures, can be found at:

<http://ajpcell.physiology.org/cgi/content/full/292/1/C115>

Additional material and information about *AJP - Cell Physiology* can be found at:

<http://www.the-aps.org/publications/ajpcell>

---

This information is current as of February 9, 2010 .

## Oxidative ATP synthesis in skeletal muscle is controlled by substrate feedback

Fan Wu,<sup>1</sup> Jeroen A. L. Jeneson,<sup>2</sup> and Daniel A. Beard<sup>1</sup>

<sup>1</sup>Biotechnology and Bioengineering Center and Department of Physiology, Medical College of Wisconsin, Milwaukee, Wisconsin; and <sup>2</sup>Biomedical NMR Laboratory, Department of Biomedical Engineering, Eindhoven University of Technology, Eindhoven, The Netherlands

Submitted 3 May 2006; accepted in final form 7 July 2006

**Wu F, Jeneson JA, Beard DA.** Oxidative ATP synthesis in skeletal muscle is controlled by substrate feedback. *Am J Physiol Cell Physiol* 292: C115–C124, 2007. First published July 12, 2006; doi:10.1152/ajpcell.00237.2006.—Data from <sup>31</sup>P-nuclear magnetic resonance spectroscopy of human forearm flexor muscle were analyzed based on a previously developed model of mitochondrial oxidative phosphorylation (*PLoS Comp Bio* 1: e36, 2005) to test the hypothesis that substrate level (concentrations of ADP and inorganic phosphate) represents the primary signal governing the rate of mitochondrial ATP synthesis and maintaining the cellular ATP hydrolysis potential in skeletal muscle. Model-based predictions of cytoplasmic concentrations of phosphate metabolites (ATP, ADP, and P<sub>i</sub>) matched data obtained from 20 healthy volunteers and indicated that as work rate is varied from rest to submaximal exercise commensurate increases in the rate of mitochondrial ATP synthesis are effected by changes in concentrations of available ADP and P<sub>i</sub>. Additional data from patients with a defect of complex I of the respiratory chain and a patient with a deficiency in the mitochondrial adenine nucleotide translocase were also predicted the by the model by making the appropriate adjustments to the activities of the affected proteins associates with the defects, providing both further validation of the biophysical model of the control of oxidative phosphorylation and insight into the impact of these diseases on the ability of the cell to maintain its energetic state.

computational model; mitochondria; cellular energetics; oxidative phosphorylation; <sup>31</sup>P-NMR spectroscopy

MITOCHONDRIAL OXIDATIVE ADP phosphorylation is the primary source of ATP in skeletal muscle during aerobic exercise. Thus, to maintain the free energy state of the cytoplasmic phosphoenergetic compounds ATP, ADP, and P<sub>i</sub>, oxidative phosphorylation is modulated to match the rate of ATP utilization during exercise. It has recently been shown through computational model-based analysis of data obtained from <sup>31</sup>P-NMR spectroscopy of working in vivo dog hearts that the primary control mechanism operating in cardiomyocytes is feedback of substrate concentrations for ATP synthesis (5). In other words, changes in the concentrations of the products generated by the utilization of ATP in the cell, ADP and P<sub>i</sub>, effect changes in the rate at which mitochondria utilize those products to resynthesize ATP (5).

Here the question of whether this same mechanism can explain the observed data on the control of oxidative metabolism in skeletal muscle is investigated. Previous analyses of <sup>31</sup>P-NMR spectroscopy (<sup>31</sup>P-MRS) data on energy balance in exercising skeletal muscle have mainly focused on testing ADP

feedback control of mitochondrial ATP synthesis using black box descriptions of the mitochondrial ATP synthetic pathway (8, 14–16, 28), P<sub>i</sub> acceptor control (7), and thermodynamic control involving quasi-linear relations between cytoplasmic Gibbs free energy of ATP hydrolysis and mitochondrial ATP synthesis flux (13, 18, 31). Yet, to date, these <sup>31</sup>P-MRS data have not been adequately explained based on a detailed mechanistic model of oxidative phosphorylation and cellular energetics.

To analyze and interpret data from skeletal muscle, our previously published model of oxidative ATP synthesis and metabolism in cardiomyocytes (5) is adapted to skeletal muscle by setting intracellular concentration pools of creatine and phosphate to appropriate values (based on measured data) and appropriately adjusting the cellular mitochondrial content to match the available morphometric data. Data on cytoplasmic ADP and P<sub>i</sub> concentrations as a function of work rate in human forearm flexor muscle from 20 untrained healthy subjects (13), 6 subjects with complex I deficiency in skeletal muscle (11, 22), and a single patient with deficiency in adenine nucleotide translocase (ANT) (2, 3) were analyzed based on the computational model.

Results of this analysis indicate that the existing computational model of the kinetics of mitochondrial oxidative phosphorylation accurately captures the in vivo kinetics of oxidative ATP synthesis and transport of phosphate metabolites between mitochondria and cytoplasm in skeletal muscle. The mechanism of control of oxidative phosphorylation is through feedback of substrates for ATP synthesis. No additional regulatory mechanisms, such as feed-forward control of certain enzymes via cytosolic calcium levels (9) or functional coupling between mitochondrial creatine kinase and ANT (23, 26, 27), are necessary to explain the majority of the observed data. In addition, the impact of specific protein deficiencies on the relationship between oxidative phosphorylation and cytoplasmic ADP and P<sub>i</sub> is successfully explained by making the appropriate modifications to the mitochondrial enzymes altered in the diseases.

### METHODS

#### Overview of Computational Model

ATP utilization, cytoplasmic phosphoenergetic buffers, and oxidative ATP synthesis are simulated in a model of skeletal muscle energetics illustrated in Fig. 1. The cell is divided into cytoplasmic and mitochondrial compartments; the variables simulated within

Address for reprint requests and other correspondence: D. A. Beard, Dept. of Physiology, Medical College of Wisconsin, 8701 Watertown Plank Rd., Milwaukee, WI 53226 (e-mail: dbeard@mcw.edu).

The costs of publication of this article were defrayed in part by the payment of page charges. The article must therefore be hereby marked “advertisement” in accordance with 18 U.S.C. Section 1734 solely to indicate this fact.

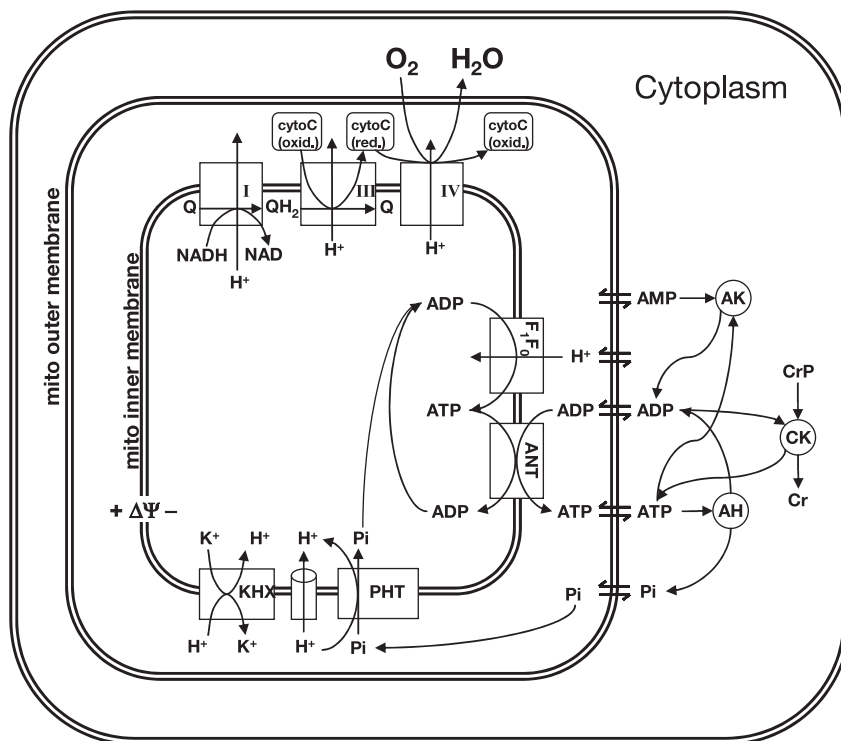


Fig. 1. Illustration of components included in the computational model of oxidative phosphorylation in skeletal muscular cells. All reactions and mass transport take place in three compartments: cytoplasm, mitochondrial intermembrane space, and mitochondrial matrix. ANT, adenine nucleotide translocase;  $\Delta\Psi$ , mitochondrial membrane potential; CK, creatine (Cr) kinase; AK, adenylate kinase; AH, (please define).

the compartments are listed in Table 1, with a brief description of the variables and units associated with each variable. The computational model for cellular energetics and oxidative phosphorylation is derived from recently published computational models developed for cardiac mitochondria (4) and cardiomyocytes (5). A complete description of the computational model is provided in the APPENDIX.

*Model Parameter Values*

Model parameter descriptions and assigned values are listed in Table 2. With the exception of the total pool of exchangeable phosphate (TPP) in the cell, all parameter values in the model are fixed at values justified by previous studies. The total exchangeable phosphate pool is computed from the equation

$$\begin{aligned}
 \text{TPP} = & [V_{\text{cyto}}W_c(2[\text{ATP}]_c + [\text{ADP}]_c + [\text{P}_i]_c + [\text{CrP}]) \\
 & + V_{\text{mito}}W_i(2[\text{ATP}]_i + [\text{ADP}]_i + [\text{P}_i]_i) \\
 & + V_{\text{mito}}W_x([\text{ATP}]_x + [\text{P}_i]_x)] \quad (1)
 \end{aligned}$$

where  $V_{\text{cyto}}$  and  $V_{\text{mito}}$  are the volume densities of cytoplasm and mitochondria in the myocyte model (in units of volume cytoplasm or mitochondria per cell volume);  $W_x$ , and  $W_i$  are the matrix and intermembrane space water volumes (in units of volume of water per volume of mitochondria), respectively; and  $W_c$  is the water fraction of the cytoplasmic space. By comparing simulation predictions with experimental data (see RESULTS), values of TPP of 36.8, 36.3, and 30.3 mM are chosen as the values most consistent with the experimental observations for healthy subjects, complex I-deficient subjects, and ANT-deficient subjects. To adjust the TPP value, the value of  $[\text{P}_i]_c$  used as an initial condition in model simulations is adjusted to obtain optimal model fits to the observed data.

The parameter values listed in Table 3 are organized structure/volume parameters, physicochemical parameters, mitochondrial model parameters, fixed concentrations and concentration pools, and binding constants.

All values for concentrations of pooled metabolites are set according to values reported in previous studies, with the exception of TPP, which is estimated below. Binding constants are obtained from the literature; enzyme activities for reactions maintained near equilibrium are set to arbitrarily high values.

<sup>31</sup>P-NMR spectroscopic measurements of phosphate metabolites in the ulnar finger flexor muscle in the human forearm were acquired at 1.5 T at rest and during voluntary ramp exercise using <sup>1</sup>H imaging-guided localization in all subjects and analyzed according to the methods described in detail elsewhere (12).

**RESULTS**

*Analysis of Data from Healthy Subjects*

Model predictions of steady-state concentrations of cytoplasmic ADP and  $\text{P}_i$  as functions of the work rate (rate of cellular ATP consumption) are compared with experimental measures obtained from healthy subjects in Fig. 2. The model predicts that ADP concentration increases from ~17  $\mu\text{M}$  at rest to ~110  $\mu\text{M}$  at the maximum observed work rate and that  $\text{P}_i$  concentration increases from 0.3 mM at rest to ~18 mM at the maximum observed work rate.

The experimental data plotted in Fig. 2 are obtained from the previous study of Jenson et al. (13). Data were collected during steady-state exercise, during which the contribution to ATP synthesis from anaerobic glycolysis was negligible (13). Cellular pH stayed within 0.1 pH units of 7.0 in all subjects. Jenson et al. (13) reported measured phosphate metabolite levels as a function of the work rate measured as a fraction of the maximal exercise rate. These fractional work rates were translated to absolute ATP synthesis fluxes based on the observations that the average rates of ATP hydrolysis in human forearm flexor muscle at rest and 65% of maximal exercise are 0.008 mmol (liter cell water)<sup>-1</sup>·s<sup>-1</sup> (6) and 0.22 mmol (liter

Table 1. *Model variables*

Variables	Description	Units
$[H^+]_x$	Concentration of $H^+$ ion in mito matrix	mol (1 matrix water) <sup>-1</sup>
$[K^+]_x$	Concentration of $K^+$ ion in mito matrix	mol (1 matrix water) <sup>-1</sup>
$[Mg^{2+}]_x$	Concentration of $Mg^{2+}$ ion in mito matrix	mol (1 matrix water) <sup>-1</sup>
$[NADH]_x$	Concentration of NADH in mito matrix	mol (1 matrix water) <sup>-1</sup>
$[NAD]_x$	Concentration of NAD in mito matrix	mol (1 matrix water) <sup>-1</sup>
$[QH_2]$	Concentration of reduced ubiquinol in mito matrix	mol (1 matrix water) <sup>-1</sup>
$[Q]$	Concentration of oxidized ubiquinol in mito matrix	mol (1 matrix water) <sup>-1</sup>
$[ATP]_x$	Concentration of total ATP in mito matrix	mol (1 matrix water) <sup>-1</sup>
$[ADP]_x$	Concentration of total ADP in mito matrix	mol (1 matrix water) <sup>-1</sup>
$[mATP]_x$	Concentration of $Mg^{2+}$ -bound ATP in mito matrix	mol (1 matrix water) <sup>-1</sup>
$[mADP]_x$	Concentration of $Mg^{2+}$ -bound ADP in mito matrix	mol (1 matrix water) <sup>-1</sup>
$[P_i]_x$	Concentration of inorganic phosphate in mito matrix	mol (1 matrix water) <sup>-1</sup>
$[cytoC(red)^{2+}]_i$	Concentration of reduced cytochrome <i>c</i> in IM space	mol (1 IM water) <sup>-1</sup>
$[cytoC(ox)^{3+}]_i$	Concentration of oxidized cytochrome <i>c</i> in IM space	mol (1 IM water) <sup>-1</sup>
$[ATP]_i$	Concentration of total ATP in IM space	mol (1 IM water) <sup>-1</sup>
$[ADP]_i$	Concentration of total ADP in IM space	mol (1 IM water) <sup>-1</sup>
$[AMP]_i$	Concentration of total AMP in IM space	mol (1 IM water) <sup>-1</sup>
$[mATP]_i$	Concentration of $Mg^{2+}$ -bound ATP in IM space	mol (1 IM water) <sup>-1</sup>
$[mADP]_i$	Concentration of $Mg^{2+}$ -bound ADP in IM space	mol (1 IM water) <sup>-1</sup>
$[P_i]_i$	Concentration of inorganic phosphate in IM space	mol (1 IM water) <sup>-1</sup>
$[Mg^{2+}]_i$	Concentration of $Mg^{2+}$ ion in IM space	mol (1 IM water) <sup>-1</sup>
$[ATP]_c$	Concentration of total ATP in myocyte	mol (1 cell water) <sup>-1</sup>
$[ADP]_c$	Concentration of total ADP in myocyte	mol (1 cell water) <sup>-1</sup>
$[AMP]_c$	Concentration of total AMP in myocyte	mol (1 cell water) <sup>-1</sup>
$[mATP]_c$	Concentration of $Mg^{2+}$ -bound ATP in myocyte	mol (1 cell water) <sup>-1</sup>
$[mADP]_c$	Concentration of $Mg^{2+}$ -bound ADP in myocyte	mol (1 cell water) <sup>-1</sup>
$[Mg^{2+}]_c$	Concentration of free $Mg^{2+}$ ion in myocyte	mol (1 cell water) <sup>-1</sup>
$[P_i]_c$	Concentration of inorganic phosphate in myocyte	mol (1 cell water) <sup>-1</sup>
$[CrP]_c$	Concentration of creatine phosphate in cytoplasm	mol (1 cell water) <sup>-1</sup>
$[Cr]_c$	Concentration of creatine in cytoplasm	mol (1 cell water) <sup>-1</sup>
$\Delta\Psi$	Mitochondrial membrane potential	mV

IM, inter membrane.

cell water)<sup>-1</sup>·s<sup>-1</sup>, respectively (14), and the assumption that power output and rate of ATP hydrolysis are linearly proportional (21).

The agreement between the model simulations and the observed data is striking considering that a single adjustable parameter (TPP) was varied to match model simulations to the data. In fact, the model-predicted  $[ADP]_c$  values are not sensitive to the value of TPP. A 10% increase in the value of this parameter results no significant change in the model predicted  $[ADP]_c$  and a >100% increase in the mean-squared difference between model predictions of  $[P_i]_c$  and the observed data. Thus the nature of the relationship between work rate and  $[ADP]_c$  does not depend on the value of TPP. The predicted  $[ADP]_c$  and  $[P_i]_c$  as a functions of workload at the value of TPP = 40.5 mM (10% greater than the optimal value) is plotted as a dashed lines in Fig. 2. It is apparent that the higher value of TPP results in an improvement in the model fit to the  $[P_i]_c$  data at low work rates, but an overall agreement between the model predictions and experimental data that is worse than for the optimal value.

To investigate the factors controlling this relationship, we analyzed the sensitivity of the model predictions of Fig. 2A to the parameter values used in the kinetic model for the ANT flux of *Eq. A10*. This expression invokes three parameters,  $X_{ANT}$ ,  $\theta$ , and  $K_{m,ADP}$  (assumed values for these parameters are listed in Table 2). To quantify the impact of variation in these parameters on the work-ADP relationship, we fit the predicted data to the function  $V = V_{max}([ADP]_c - x_o)/([ADP]_c - x_o + K_m)$ , where  $V$  represents the ATPase flux and  $V_{max}$ ,  $x_o$ , and  $K_m$  are fitting parameters. The predictions plotted in Fig. 2A are

well represented by this function for  $V_{max} = 0.44$  mmols<sup>-1</sup> (1 cell)<sup>-1</sup>,  $x_o = 16.5$   $\mu$ M, and  $K_m = 0.11$  mM. Sensitivity analysis reveals that the apparent  $K_m$  is highly sensitive to the value of  $\theta$  (sensitivity coefficient  $|\partial \ln K_m / \partial \ln \theta| \approx 5$ ), and less sensitive to  $X_{ANT}$  (sensitivity coefficient  $|\partial \ln K_m / \partial \ln X_{ANT}| \approx 0.5$ ). The  $V_{max}$  is most sensitive to the value of  $X_{ANT}$  (sensitivity coefficient  $|\partial \ln V_{max} / \partial \ln X_{ANT}| \approx 0.6$ ) and less sensitive to  $\theta$  (sensitivity coefficient  $|\partial \ln V_{max} / \partial \ln \theta| \approx 0.3$ ). Neither  $K_m$  nor  $V_{max}$  is sensitive to the value of  $K_{m,ADP}$ . Thus, in terms of the ANT transporter model, the apparent  $K_m$  for the relationship between ADP and work is primarily controlled by the parameter  $\theta$ .

#### *Analysis of Data from Patients with Complex I Deficiency*

Model predictions and experimental data from six patients (three of which were first- and second-degree relatives) who were diagnosed with mitochondrial complex I deficiency at the isolated mitochondria level are plotted in Fig. 3. These data were collected under the same protocol as for the healthy subjects; data were first published in Ref. 11. The experimental data show steeper relationships between  $[ADP]_c$  (or  $[P_i]_c$ ) and ATP hydrolysis rate than are observed in healthy subjects, resulting from an impaired capacity of the mitochondria to synthesize ATP and transport it to the cytoplasm as levels of ADP and  $P_i$  increase.

To match the observed data on complex I-deficient patients, the mitochondrial model was modified in two ways. First, based on observations that whole-body resting oxygen

Table 2. *Parameter values*

Parameter	Description	Value	Units	Reference
<b>Physicochemical Parameters</b>				
$RT$	Gas constant times temperature	2.5775	$\text{kJ mol}^{-1}$	
$F$	Faraday's constant	0.096484	$\text{kJ mol}^{-1} \text{mV}^{-1}$	
$\Delta G_{o,C1}$	Standard free energy, complex I	-69.37	$\text{kJ mol}^{-1}$	1 <sup>a</sup>
$\Delta G_{o,C3}$	Standard free energy, complex III	-32.53	$\text{kJ mol}^{-1}$	1 <sup>a</sup>
$\Delta G_{o,C4}$	Standard free energy, complex IV	-122.94	$\text{kJ mol}^{-1}$	1 <sup>a</sup>
$\Delta G_{o,ATP}$	Standard free energy, ATPase	36.03	$\text{kJ mol}^{-1}$	1 <sup>a</sup>
<b>Structure/Volume Parameters</b>				
$V_{\text{cyto}}$	Cytoplasm volume	0.894	(1 cytoplasm) (1 cell) <sup>-1</sup>	
$V_{\text{mito}}$	Mitochondrial volume	0.056	(1 mito) (1 cell) <sup>-1</sup>	30
$W_x$	Matrix water space fraction	0.6514	(1 water) (1 mito) <sup>-1</sup>	4, 29
$W_i$	IM space water fraction	0.0724	(1 water) (1 mito) <sup>-1</sup>	4, 29
$W_c$	Cytoplasm water fraction	0.8425	(1 water) (1 cytoplasm) <sup>-1</sup>	29
$\gamma$	Outer membrane area per mito volume	5.99	$\mu\text{m}^{-1}$	20
<b>Mitochondrial Models</b>				
$r$	Dehydrogenase model parameter	4.559	unitless	5 <sup>c</sup>
$k_{\text{Pi},1}$	Dehydrogenase model parameter	0.1553	mM	5 <sup>c</sup>
$k_{\text{Pi},2}$	Dehydrogenase model parameter	0.8222	mM	5 <sup>c</sup>
$X_{\text{DH}}$	Dehydrogenase activity	0.0866	$\text{mol s}^{-1} \text{M}^{-1}$ (1 mito) <sup>-1</sup>	5 <sup>c</sup>
$X_{\text{C1}}$	Complex I activity	$4.405 \times 10^3$	$\text{mol s}^{-1} \text{M}^{-2}$ (1 mito) <sup>-1</sup>	5 <sup>bc</sup>
$X_{\text{C3}}$	Complex III activity	4.887	$\text{mol s}^{-1} \text{M}^{-3/2}$ (1 mito) <sup>-1</sup>	5 <sup>c</sup>
$X_{\text{C4}}$	Complex IV activity	$6.766 \times 10^{-5}$	$\text{mol s}^{-1} \text{M}^{-1}$ (1 mito) <sup>-1</sup>	5 <sup>c</sup>
$X_{\text{F1}}$	$F_1 F_0$ -ATPase activity	1,000	$\text{mol s}^{-1} \text{M}^{-1}$ (1 mito) <sup>-1</sup>	5 <sup>c</sup>
$X_{\text{ANT}}$	ANT activity	$8.123 \times 10^{-3}$	$\text{mol s}^{-1}$ (1 mito) <sup>-1</sup>	5 <sup>bc</sup>
$X_{\text{PiHt}}$	$\text{H}^+/\text{P}_i^-$ co-transport activity	$3.850 \times 10^5$	$\text{mol s}^{-1} \text{M}^{-1}$ (1 mito) <sup>-1</sup>	5 <sup>c</sup>
$k_{\text{PiHt}}$	$\text{H}^+/\text{P}_i^-$ co-transport parameter	0.2542	mM	5 <sup>c</sup>
$X_{\text{KH}}$	$\text{K}^+/\text{H}^+$ antiporter activity	$5.651 \times 10^7$	$\text{mol s}^{-1} \text{M}^{-2}$ (1 mito) <sup>-1</sup>	5 <sup>c</sup>
$X_{\text{Hle}}$	Proton leak activity	200.00	$\text{mol s}^{-1} \text{M}^{-1} \text{mV}^{-1}$ (1 mito) <sup>-1</sup>	5 <sup>c</sup>
$k_{\text{Pi},3}$	Complex III/ $\text{P}_i$ parameter	0.3601	mM	5 <sup>c</sup>
$k_{\text{Pi},4}$	Complex III/ $\text{P}_i$ parameter	5.924	mM	5 <sup>c</sup>
$n_A$	$\text{H}^+$ stoich. coef. for $F_1 F_0$ -ATPase	3	unitless	24
$P_{\text{Pi}}$	Mitochondrial membrane permeability to inorganic phosphate	327	$\mu\text{m/s}$	26
$P_A$	Mitochondrial outer membrane permeability to nucleotides	85.0	$\mu\text{m/s}$	17
$k_{\text{m,ADP}}$	ANT Michaelis-Menten constant	$3.5 \times 10^6$	M	26 <sup>c</sup>
$\theta$	ANT parameter	0.35	unitless	26 <sup>c</sup>
$k_{\text{O2}}$	Kinetic constant for complex IV	$1.2 \times 10^{-4}$	M	26 <sup>c</sup>
$\beta$	Matrix buffering capacity	0.01	M	26 <sup>c</sup>
$C_{\text{IM}}$	Capacitance of inner membrane	$6.75 \times 10^{-6}$	$\text{mol (1 mito)}^{-1} \text{mV}^{-1}$	4, 10
<b>Fixed Concentrations and Concentration Pools</b>				
$\text{NAD}_{\text{tot}}$	Total matrix NAD(H) concentration	2.97	$\text{mol (1 matrix water)}^{-1}$	26 <sup>c</sup>
$Q_{\text{tot}}$	Total matrix ubiquinol concentration	1.35	$\text{mol (1 matrix water)}^{-1}$	26 <sup>c</sup>
$\text{cytC}_{\text{tot}}$	Total IM cytochrome <i>c</i> concentration	2.70	$\text{mol (1 IM water)}^{-1}$	26 <sup>c</sup>
$A_{\text{tot}}$	Total matrix ATP + ADP concentration	10	$\text{mol (1 matrix water)}^{-1}$	26 <sup>c</sup>
$[\text{H}^+]_c$	$\text{H}^+$ ion concentration in cytoplasm	$10^{-7.0}$	$\text{mol (1 cytoplasm water)}^{-1}$	
$[\text{K}^+]_c$	$\text{K}^+$ ion concentration in cytoplasm	150	$\text{mol (1 cytoplasm water)}^{-1}$	
TPP	Total phosphate pool	30.3–36.8	$\text{mmol (1 cell)}^{-1}$	
$\text{CR}_{\text{tot}}$	Total Cr + CrP concentration	42.7	$\text{mol (1 cytoplasm water)}^{-1}$	13
$[\text{O}_2]$	Oxygen concentration	$3.48 \times 10^{-5}$	M	
<b>Binding Constants</b>				
$K_{\text{AK}}$	Adenylate kinase equilibrium constant	0.4331	unitless	1 <sup>a</sup>
$K_{\text{CK}}$	Creatine kinase equilibrium constant	$1.66 \times 10^9$	$\text{M}^{-1}$	25
$K_{\text{Mg-ATP}}$	Mg-ATP binding constant	$24 \times 10^{-6}$	M	26
$K_{\text{Mg-ADP}}$	Mg-ADP binding constant	$347 \times 10^{-6}$	M	26
$X_{\text{AK}}$	Adenylate kinase activity	$1 \times 10^7$	$\text{M s}^{-1} \text{M}^{-2}$	
$X_{\text{CK}}$	Creatine kinase activity	$1 \times 10^{-7}$	$\text{M s}^{-1} \text{M}^{-2}$	
$X_{\text{MgA}}$	$\text{Mg}^{2+}$ binding activity	$1 \times 10^{-7}$	$\text{M s}^{-1} \text{M}^{-2}$	
$k_{\text{dH}}$	$\text{H}_2\text{PO}_4^-$ proton dissociate constant	$1.7783 \times 10^{-7}$	M	1

TPP values have been adjusted to match data. <sup>a</sup>Computed from thermodynamic data tabulated in cited reference. <sup>b</sup>Value is for control (healthy) subjects. <sup>c</sup>Value used is taken from previous modeling studies, not direct experimental measure.

consumption is increased in the patients with complex I deficiency compared with healthy subjects (22), it was assumed that no protons are pumped by complex I, altering the stoichiometry of the reaction model. Changes to the governing equations to account for this phenomenon are

described in the APPENDIX; see *Eq. A19* for details. This change in the proton stoichiometry results in a 47% increase in the predicted rate of resting oxygen consumption in the muscle compared with the normal (healthy) case. Measured whole-body resting oxygen consumption in three patients

Table 3. *Model fluxes*

Flux	Description	Units
<i>Mitochondrial Matrix Reactions</i>		
$J_{DH}$	Mitochondrial dehydrogenase	$\text{mol s}^{-1} (1 \text{ mito})^{-1}$
$J_{C1}$	Complex I	$\text{mol s}^{-1} (1 \text{ mito})^{-1}$
$J_{C3}$	Complex III	$\text{mol s}^{-1} (1 \text{ mito})^{-1}$
$J_{C4}$	Complex IV	$\text{mol s}^{-1} (1 \text{ mito})^{-1}$
$J_{F1}$	$F_1F_0$ ATPase reaction	$\text{mol s}^{-1} (1 \text{ mito})^{-1}$
$J_{ANT}$	Adenine nucleotide translocase	$\text{mol s}^{-1} (1 \text{ mito})^{-1}$
$J_{PiHt}$	Phosphate-hydrogen cotransporter	$\text{mol s}^{-1} (1 \text{ mito})^{-1}$
$J_{Hle}$	Proton leak	$\text{mol s}^{-1} (1 \text{ mito})^{-1}$
$J_{KH}$	Mitochondrial $K^+/H^+$ exchanger	$\text{mol s}^{-1} (1 \text{ mito})^{-1}$
$J_{MgATPx}$	$Mg^{2+}/ATP$ binding in matrix	$\text{mol s}^{-1} (1 \text{ mito})^{-1}$
$J_{MgADPx}$	$Mg^{2+}/ADP$ binding in matrix	$\text{mol s}^{-1} (1 \text{ mito})^{-1}$
<i>Mitochondrial IM Space Reactions</i>		
$J_{AKi}$	Adenylate kinase flux in IM space	$\text{mol s}^{-1} (1 \text{ mito})^{-1}$
$J_{MgATPi}$	$Mg^{2+}/ATP$ binding in IM space	$\text{mol s}^{-1} (1 \text{ mito})^{-1}$
$J_{MgADPi}$	$Mg^{2+}/ADP$ binding in IM space	$\text{mol s}^{-1} (1 \text{ mito})^{-1}$
<i>Mitochondrial Transport Fluxes</i>		
$J_{Pit}$	Phosphate transport across outer membrane	$\text{mol s}^{-1} (1 \text{ mito})^{-1}$
$J_{ATPt}$	ATP transport across outer membrane	$\text{mol s}^{-1} (1 \text{ mito})^{-1}$
$J_{ADPt}$	ADP transport across outer membrane	$\text{mol s}^{-1} (1 \text{ mito})^{-1}$
$J_{AMPt}$	AMP transport across outer membrane	$\text{mol s}^{-1} (1 \text{ mito})^{-1}$
<i>Cytoplasmic Reactions</i>		
$J_{AKc}$	Adenylate kinase flux in cytoplasm	$\text{mol s}^{-1} (1 \text{ cytoplasm})^{-1}$
$J_{CKc}$	Creatine kinase flux in cytoplasm	$\text{mol s}^{-1} (1 \text{ cytoplasm})^{-1}$
$J_{MgATPc}$	$Mg^{2+}/ATP$ binding in cytoplasm	$\text{mol s}^{-1} (1 \text{ cytoplasm})^{-1}$
$J_{MgADPc}$	$Mg^{2+}/ADP$ binding in cytoplasm	$\text{mol s}^{-1} (1 \text{ cytoplasm})^{-1}$
$J_{AIC}$	ATP consumption in cytoplasm	$\text{mol s}^{-1} (1 \text{ cell})^{-1}$

with this deficiency was  $28 \pm 14\%$  greater compared with healthy subjects (22). Second, the activity of complex I was reduced to  $\sim 1/1,000$  of the normal value to match the observed data. Thus, to obtain the model predictions illustrated in Fig. 3, the activity of complex I was reduced by approximate 1,000-fold compared with the normal case.

Here the model shows excellent agreement to the observed data on both  $[ADP]_c$  and  $[P_i]_c$ . As is the case for the data from healthy subjects, the predictions of  $[P_i]_c$  are sensitive to the value of TPP, whereas the predictions of  $[ADP]_c$  are not. Thus the relationship between work rate and substrates for ATP synthesis is explained by a drastic reduction in the activity and a loss in proton pumping of mitochondrial complex I.

#### *Analysis of Data from Patient with ANT Deficiency*

Figure 4 shows data on  $[ADP]_c$  and  $[P_i]_c$  measured in a single patient characterized as having an ANT deficiency in muscle (2, 3). The ANT transporter exchanges mitochondrial ATP for cytoplasmic ADP. Thus impairment in the activity of ANT results in a reduction in the ability of the mitochondrion to deliver ATP to the cytoplasm. Data were collected under the protocol described for healthy and complex I-deficient subjects; a subset of these data was first published in Ref. 11.

Western blot analysis revealed that in the patient the ANT protein was present at 25% of the concentration found in healthy subjects (3). Thus to account for the deficiency in the model, the activity of the ANT transporter was reduced to 25% of the normal value for healthy subjects.

Figure 4 shows that ADP was much higher at rest and increased more rapidly with exercise in this patient than in healthy subjects and in the complex I-deficient patients. The ADP concentration of  $150 \mu\text{M}$  that was measured at the modest work rate of  $0.081 \text{ mmol ATP consumed per second per liter cell}$  was greater than any value measured in the healthy or complex I deficient subjects. Model predictions are similar to the measured data; the model predicts  $[ADP]_c$  is  $42 \mu\text{M}$  at rest (compared with the measured value of  $64 \mu\text{M}$ ) and increases sharply with work rate.

*Maintenance of free energy of ATP hydrolysis.* Figure 5 shows model-predicted free energy of ATP hydrolysis vs. ATP hydrolysis rate, computed using the parameters obtained for the healthy subjects, complex I-deficient patients, and the ANT deficient patient. Since cellular pH values are  $7.0 \pm 0.1$  for all the subjects, the free energy of ATP hydrolysis is computed by the relationship

$$\Delta G_{ATP} = \Delta G_{o,ATP} + RT \ln \left( \frac{[fADP]_c [Pi]_c}{[fATP]_c} \right) \quad (2)$$

where  $\Delta G_{ATP}$  is the standard free energy of ATP hydrolysis at pH 7.0,  $R$  is the universal gas constant, and  $T$  is temperature in degrees Kelvin (for parameter values, see Table 2).  $[fADP]_c$  and  $[fATP]_c$  denote magnesium unbound ADP and ATP concentration in the cytoplasm, respectively. For the normal subjects, Jeneson et al. (9) observed quasi-linear relationship between the free energy of ATP hydrolysis and power output; the model predictions verify this observation except at low work rates where the predicted values of  $[P_i]_c$  tend to be lower than the observed values.

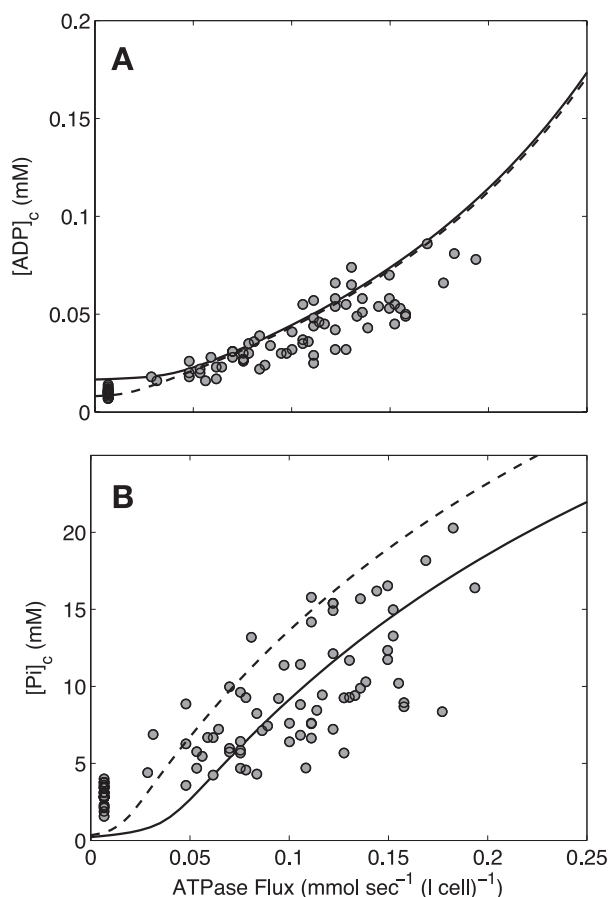


Fig. 2. Model prediction of ADP concentration and inorganic phosphate concentration in cytoplasm as a function of ATP hydrolysis rate in the healthy subjects. *A*: plot of predicted ADP concentration in cytoplasm,  $[ADP]_c$ , as a function of ATP hydrolysis rate, ATPase flux. *B*: plot of predicted  $P_i$  concentration in cytoplasm,  $[P_i]_c$ , as a function of ATP hydrolysis rate, ATPase flux. The solid and dashed lines represent model-predicted results. The circles represent experimentally measured estimation from Jenson et al. (9). Solid line correspond to the optimal value of the total pool of exchangeable phosphate (TPP) = 36.8 mM; dashed lines correspond to TPP = 40.5 mM (10% greater than the optimal value).

## DISCUSSION

This work introduces an integrated computational model for skeletal muscle oxidative phosphorylation and fluxes of ATP, ADP, AMP, CrP, and  $P_i$  in the cytoplasm. Although the central component of the model—mitochondrial oxidative phosphorylation—is based on a mitochondrial model previously developed to match data on isolated mitochondria from rat heart, the integrated model matches a rich set of data on in vivo phosphate compounds from human skeletal muscle in healthy and complex I deficient individuals. The model also produces reasonable predictions for the ANT deficient subject, although the data available for comparison are sparse.

The analysis predicts that the rate of oxidative phosphorylation is primarily regulated through concentrations of the substrates for ATP synthesis (ADP and  $P_i$ ), since no additional control mechanisms, such as feed-forward control of certain enzymes via cytosolic calcium levels (9) and functional coupling between mitochondrial creatine kinase and ANT (23, 26, 27) that have been proposed to operate in the heart, were incorporated into the model. The current analysis does not rule

out the possibility that ancillary control mechanisms are active in skeletal muscle (16, 28); however, it shows that major contributions of such mechanisms to the overall regulation of the mitochondrial ATP synthetic pathway are not necessary to explain the thrust of the observed data.

Although the model predicts cytoplasmic ADP,  $P_i$ , and ATP (not shown) concentrations that agree well with observed data, the present model systematically underpredicts  $P_i$  concentration in the resting state. As illustrated in Fig. 2*B*,  $^{31}P$  MRS measurements indicate that inorganic phosphate concentrations are  $\sim 3$  mM at rest, whereas the model predicts resting  $[P_i]_c$  to be only 0.3 mM. This may be due in part to the fact that the mitochondrial model was constructed to match data obtained from mitochondria isolated from cardiomyocytes. Inorganic phosphate concentrations in heart are significantly lower than in mixed fiber type skeletal muscle such as human skeletal muscle (19) if not undetectable at low work rates (32).

We used the empirical fitting function  $V = V_{max}([ADP]_c - x_o)/([ADP]_c - x_o + K_m)$  to capture key trends in the model prediction for the control case and to characterize the sensitivity of the model predictions to key model parameters in terms of sensitivity coefficients for the fitting parameters. Sensitivity analysis revealed that the parameter  $\theta$  for ANT flux in the

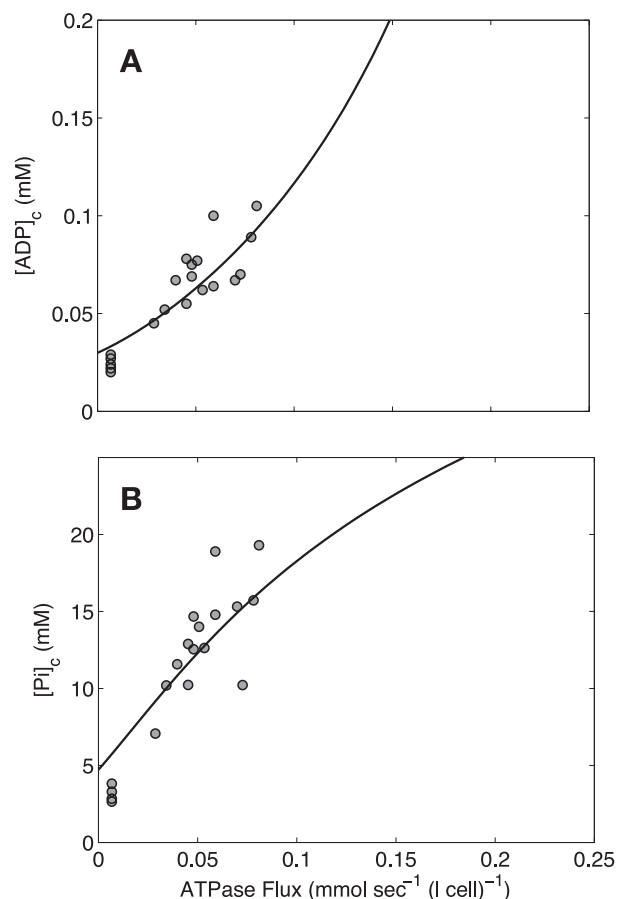


Fig. 3. Model prediction of ADP concentration and inorganic phosphate concentration in cytoplasm as a function of ATP hydrolysis rate in the complex I-deficient subjects. *A*: plot of predicted ADP concentration in cytoplasm as a function of ATP hydrolysis rate, ATPase flux. *B*: plot of predicted  $P_i$  concentration in cytoplasm as a function of ATP hydrolysis rate, ATPase flux. The solid line represents model-predicted results. The circle points represent experimentally measured estimation from Jenson et al. (8).

model has a significant impact on the apparent affinity for ADP in the relationship between cytoplasmic ADP concentration and rate of oxidative metabolism. Future studies including a full-scale sensitivity and metabolic control analysis of the current model as well as next-generation models incorporating ancillary biochemical detail will be necessary to further improve agreement of predicted data with empirical knowledge.

The control of oxidative phosphorylation by substrate concentrations allows the mitochondria to maintain a free energy of ATP hydrolysis of less than  $-55$  kJ/mol over the observed range of work rates in human forearm muscle of healthy subjects. However, as shown in Fig. 5, the magnitude of  $\Delta G_{\text{ATP}}$  drops more quickly with increasing work in the ANT-deficient patients than in normal subjects, and the predicted magnitude of  $\Delta G_{\text{ATP}}$  in the complex I-deficient patients at rest is significantly lower than that of the other two sets of subjects. These abnormalities in the complex I- and ANT-deficient subjects result in reduced capacity to do work.

Data on complex I-deficient patients are fit by reducing the activity of complex I compared with the normal case, and assuming that complex I pumps no protons in the complex I deficient patients. However, while the closest fit to the ob-

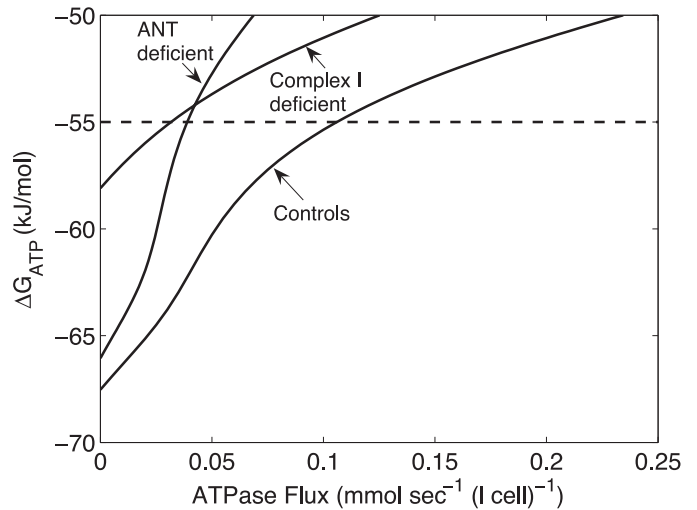


Fig. 5. Model-generated curves of free energy of ATP hydrolysis against ATP hydrolysis rate for the healthy subjects, the complex I-deficient subjects, and the ANT-deficient subjects. The free energy of ATP hydrolysis,  $\Delta G_{\text{ATP}}$ , is computed based on model-predicted concentrations of metabolites in cytoplasm. The dashed line corresponds to a  $\Delta G_{\text{ATP}}$  value of  $-55$  kJ/mol.

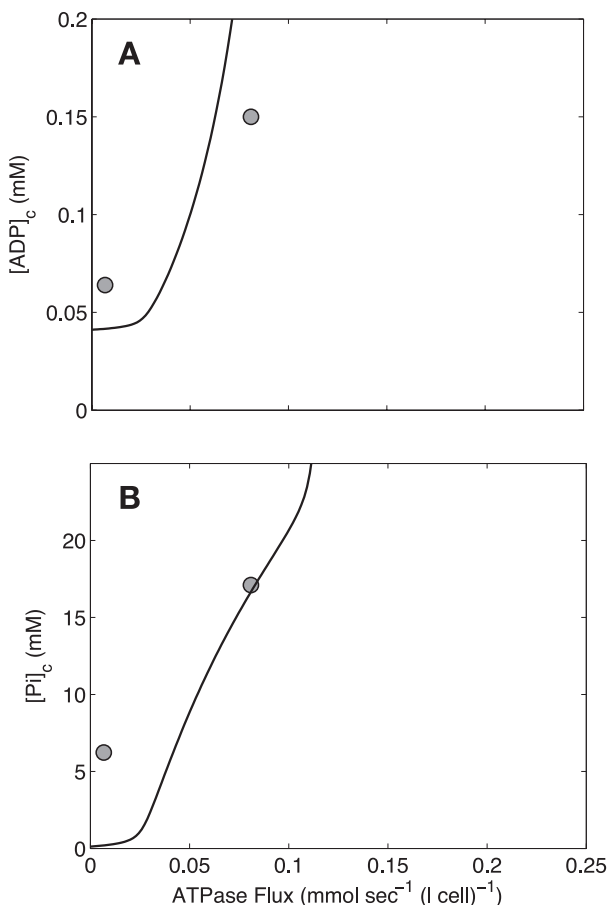


Fig. 4. Model prediction of ADP concentration and inorganic phosphate concentration in cytoplasm as a function of ATP hydrolysis rate in the ANT-deficient subjects. A: plot of predicted ADP concentration in cytoplasm as a function of ATP hydrolysis rate, ATPase flux. B: plot of predicted inorganic phosphate concentration in cytoplasm as a function of ATP hydrolysis rate, ATPase flux. The solid line represents model-predicted results. The circles represent experimentally measured estimation from Bakker et al. (3).

erved data on ADP and  $P_i$  is obtained by reducing the complex I activity by a factor of  $\sim 1/1,000$  compared with the normal case, it is necessary to be cautious in interpreting the scaling factor of  $\sim 1/1,000$ . Since the complex I activity for the normal case was not identified with significant sensitivity (4), the ratio between activities in normal and complex I deficient patients also cannot be determined sensitively. Yet, regardless of the sensitivity of the estimate, it was clear from oxygen polarographic studies on isolated mitochondria from patient leg muscle biopsies (H. R. Scholte, unpublished observations) that the activity of complex I is significantly diminished in the complex I deficient patients.

To analyze data from the patient with a deficiency of ANT, it was not necessary to introduce an arbitrary scaling factor to fit the measured data. Since the level of ANT expressed in mitochondria of the patient was directly assayed and found to be 25% of that in healthy subjects, it was possible to incorporate this measurement directly in the model by scaling the healthy ANT activity by 0.25. The fact that differences observed in cytoplasmic phosphoenergetic compounds between healthy subjects and this patient are explained based on this single adjustment to the model provides independent validation of the mitochondrial model and the conclusions drawn from its behavior.

## APPENDIX

### Computational Model

The computational model for skeletal muscle energetics and oxidative phosphorylation is derived from a previously published model applied to cardiac tissue (5). For the current application, the cardiac model has been modified in two ways to adapt the model to analyze data from human skeletal muscle. First, the oxygen transport component of the previous model has been removed. It is assumed that the skeletal muscle remains normoxic during the experiments and the cellular oxygen concentration,  $[O_2]$ , which is a variable in the model of Beard (5), appears as a fixed parameter in the current model. Second, the mitochondrial volume of the muscle cell, which is  $\sim 30\%$  of cell volume in cardiomyocytes (29), is set to  $V_{\text{mito}} = 0.056$  (l mito)

(l cell)<sup>-1</sup>, a value measured from biopsies of human vastus lateralis muscle (30).

The model is expressed in terms of the following set of differential equations:

$$\begin{aligned}
 d[\text{H}^+]_x/dt &= \beta^{-1}[\text{H}^+]_x(+J_{\text{DH}} - 5J_{\text{C1}} - 2J_{\text{C3}} - 4J_{\text{C4}} + (n_A - 1)J_{\text{F1}} \\
 &\quad + 2J_{\text{Pit}} - J_{\text{KH}} + J_{\text{Hic}})/W_x \\
 d[\text{K}^+]_x/dt &= (+J_{\text{KH}})/W_x \\
 d[\text{Mg}^{2+}]_x/dt &= (-J_{\text{MgADP}_x} - J_{\text{MgATP}_x})/W_x \\
 d[\text{NADH}]_x/dt &= (+J_{\text{DH}} - J_{\text{C1}})/W_x \\
 d[\text{QH}_2]_x/dt &= (+J_{\text{C1}} - J_{\text{C3}})/W_x \\
 d[\text{cytC}(\text{red})^{2+}]_i/dt &= (+2J_{\text{C3}} - 2J_{\text{C4}})/W_i \\
 d[\text{ATP}]_x/dt &= (+J_{\text{P1}} - J_{\text{ANT}})/W_x \\
 d[\text{mATP}]_x/dt &= (+J_{\text{MgATP}_x})/W_x \\
 d[\text{mADP}]_x/dt &= (+J_{\text{MgADP}_x})/W_x \\
 d[\text{P}_i]_x/dt &= (-J_{\text{F1}} + J_{\text{Pit}})/W_x \\
 d[\text{ATP}]_i/dt &= (+J_{\text{ATP}_i} + J_{\text{ANT}} + J_{\text{AKi}})/W_i \\
 d[\text{ADP}]_i/dt &= (+J_{\text{ADP}_i} - J_{\text{ANT}} - 2J_{\text{AKi}})/W_i \\
 d[\text{AMP}]_i/dt &= (+J_{\text{AMP}_i} + J_{\text{AKi}})/W_i \\
 d[\text{mATP}]_i/dt &= (+J_{\text{MgATP}_i})/W_i \\
 d[\text{mADP}]_i/dt &= (+J_{\text{MgADP}_i})/W_i \\
 d[\text{Pi}]_i/dt &= (+J_{\text{Pit}} - J_{\text{Pit}})/W_i \\
 d[\text{Mg}^{2+}]_i/dt &= (-J_{\text{MgADP}_i} - J_{\text{MgATP}_i})/W_i \\
 d[\text{ATP}]_c/dt &= [-(V_{\text{mito}}/V_{\text{cyto}})J_{\text{ATP}_c} - J_{\text{Aic}}/V_{\text{cyto}} + J_{\text{AKc}} + J_{\text{CKc}}]/W_c \\
 d[\text{ADP}]_c/dt &= [-(V_{\text{mito}}/V_{\text{cyto}})J_{\text{ADP}_c} + J_{\text{Aic}}/V_{\text{cyto}} - 2J_{\text{AKc}} - J_{\text{CKc}}]/W_c \\
 d[\text{AMP}]_c/dt &= [-(V_{\text{mito}}/V_{\text{cyto}})J_{\text{AMP}_c} + J_{\text{AKc}}]/W_c \\
 d[\text{MgATP}]_c/dt &= (+J_{\text{MgATP}_c})/W_c \\
 d[\text{MgADP}]_c/dt &= (+J_{\text{MgADP}_c})/W_c \\
 d[\text{P}_i]_c/dt &= [-(V_{\text{mito}}/V_{\text{cyto}})J_{\text{Pit}} + J_{\text{Aic}}/V_{\text{cyto}}]/W_c \\
 d[\text{Mg}^{2+}]_c/dt &= (-J_{\text{MgADP}_c} - J_{\text{MgATP}_c})/W_c \\
 d[\text{CrP}]_c/dt &= (-J_{\text{CKc}})/W_c \\
 d\Delta\psi/dt &= (+4J_{\text{C1}} + 2J_{\text{C3}} + 4J_{\text{C4}} - n_A J_{\text{F1}} - J_{\text{ANT}} - J_{\text{Hic}})/C_{\text{IM}}
 \end{aligned}
 \tag{A1}$$

In the above set of equations, the subscripts “x”, “i”, and “c”, denote mitochondrial matrix, intermembrane space, and cytoplasm, respectively. All of the variables in this set of equations are defined in Table 1.

In addition to the state variables treated in Eq. (A1), the concentrations of several species are computed

$$\begin{aligned}
 \text{NAD}_x &= \text{NAD}_{\text{tot}} - [\text{NADH}]_x \\
 [\text{Q}] &= \text{Q}_{\text{tot}} - [\text{QH}_2] \\
 [\text{cytC}(\text{ox})^{3+}]_i &= \text{cytC}_{\text{tot}} - [\text{cytC}(\text{red})^{2+}]_i \\
 [\text{ADP}]_x &= \text{A}_{\text{tot}} - [\text{ATP}]_x \\
 [\text{Cr}]_c &= \text{CR}_{\text{tot}} - [\text{CrP}]_c
 \end{aligned}
 \tag{A2}$$

where  $\text{NAD}_{\text{tot}}$ ,  $\text{Q}_{\text{tot}}$ ,  $\text{cytC}_{\text{tot}}$ , and  $\text{A}_{\text{tot}}$ , are the total concentrations of NAD(H), ubiquinol, cytochrome *c*, and adenine nucleotide in the matrix, respectively, and  $\text{CR}_{\text{tot}}$  is the total creatine plus creatine phosphate concentration in the cytoplasm.

Parameters that appear in the above equations are described in detail below. The fluxes that appear on the right-hand side of the governing equations are tabulated in Table 2. For mitochondrial species, the governing equations follow from Ref. 4. For cytoplasmic species, the reactions modeled are ATP consumption, creatine kinase reaction, adenylate kinase reaction, and transport between the cytoplasm and the mitochondrial intermembrane space.

### Mathematical Expressions for Mitochondrial Fluxes

The expressions for the mitochondrial fluxes in the model are described in detail in Ref. 4, and are listed here without detailed explanations. Definitions of the variables and parameters that appear in the following expressions are listed in Tables 2 and 3.

Dehydrogenase flux:

$$J_{\text{DH}} = X_{\text{DH}} \left( \frac{1 + [\text{P}_i]_x/k_{\text{P1,1}}}{1 + [\text{P}_i]_x/k_{\text{P1,2}}} \right) (r[\text{NAD}]_x - [\text{NADH}]_x)
 \tag{A3}$$

Complex I flux

$$J_{\text{C1}} = X_{\text{C1}} \{ e^{-[\Delta G_{\text{C1}} + 4\Delta G_{\text{H}} - RT \ln([\text{H}^+]_x/10^{-7})]/RT} [\text{NADH}]_x [\text{Q}] - [\text{NAD}]_x [\text{QH}_2] \}
 \tag{A4}$$

Where  $\Delta G_{\text{H}} = F\Delta\psi + RT \ln([\text{H}^+]_c/[\text{H}^+]_x)$ .

Complex III flux

$$\begin{aligned}
 J_{\text{C3}} &= X_{\text{C3}} \left( \frac{1 + [\text{P}_i]_x/k_{\text{P1,3}}}{1 + [\text{P}_i]_x/k_{\text{P1,4}}} \right) \cdot (e^{-[\Delta G_{\text{C3}} + 4\Delta G_{\text{H}} - 2F\Delta\psi]/2RT} \\
 &\quad \times [\text{cytC}(\text{ox})^{3+}]_i [\text{QH}_2]^{1/2} - [\text{cytC}(\text{red})^{2+}]_i [\text{Q}]^{1/2})
 \end{aligned}
 \tag{A5}$$

Complex IV flux

$$\begin{aligned}
 J_{\text{C4}} &= X_{\text{C4}} \left( \frac{[\text{O}_2]}{[\text{O}_2] + k_{\text{O}_2}} \right) \frac{[\text{cytC}(\text{red})^{2+}]_i}{\text{cytC}_{\text{tot}}} \\
 &\quad \times \{ e^{-[\Delta G_{\text{C4}} + 2G_{\text{H}} - 2RT \Delta \ln([\text{H}^+]_x/10^{-7})]/2RT} \\
 &\quad \times [\text{cytC}(\text{red})^{2+}]_i [\text{O}_2]^{1/4} - e^{+F\Delta\psi/RT} [\text{cytC}(\text{ox})^{3+}]_i \}
 \end{aligned}
 \tag{A6}$$

where  $[\text{O}_2]$  is the  $\text{O}_2$  concentration in the cell, which is set at the fixed constant of  $3.48 \times 10^{-5}$  M.

$\text{F}_1\text{F}_0$ -ATPase flux

$$J_{\text{F1}} = X_{\text{F1}} \left\{ e^{-[\Delta G_{\text{b,ATP}} - n_A \Delta G_{\text{H}}]/RT} \frac{K_{\text{Mg-ADP}}}{K_{\text{Mg-ATP}}} [\text{mADP}]_x [\text{P}_i]_x - (1\text{M})[\text{mATP}]_x \right\}
 \tag{A7}$$

Magnesium binding fluxes

$$\begin{aligned}
 J_{\text{MgATP}_x} &= X_{\text{MgA}} ([\text{fATP}]_x [\text{Mg}^{2+}]_x - K_{\text{Mg-ATP}} [\text{mATP}]_x) \\
 J_{\text{MgADP}_x} &= X_{\text{MgA}} ([\text{fADP}]_x [\text{Mg}^{2+}]_x - K_{\text{Mg-ADP}} [\text{mADP}]_x) \\
 J_{\text{MgATP}_i} &= X_{\text{MgA}} ([\text{fATP}]_i [\text{Mg}^{2+}]_i - K_{\text{Mg-ATP}} [\text{mATP}]_i) \\
 J_{\text{MgADP}_i} &= X_{\text{MgA}} ([\text{fADP}]_i [\text{Mg}^{2+}]_i - K_{\text{Mg-ADP}} [\text{mADP}]_i)
 \end{aligned}
 \tag{A8}$$

where  $[\text{fATP}]_x$ ,  $[\text{fADP}]_x$ ,  $[\text{fATP}]_i$ , and  $[\text{fADP}]_i$  denote magnesium unbound ATP in the matrix, ADP in the matrix, ATP in the intermembrane space, and ADP in the intermembrane space, respectively.

Substrate transport fluxes

$$\begin{aligned}
 J_{\text{ATP}_i} &= \gamma P_A ([\text{ATP}]_c - [\text{ATP}]_i) \\
 J_{\text{ADP}_i} &= \gamma P_A ([\text{ADP}]_c - [\text{ADP}]_i) \\
 J_{\text{AMP}_i} &= \gamma P_A ([\text{AMP}]_c - [\text{AMP}]_i) \\
 J_{\text{Pit}} &= \gamma P_i ([\text{Pi}]_c - [\text{Pi}]_i)
 \end{aligned}
 \tag{A9}$$

Adenine nucleotide translocase (ANT) flux

$$J_{\text{ANT}} = X_{\text{ANT}} \left( \frac{[\text{fADP}]_i}{[\text{fADP}]_i + [\text{fATP}]_i e^{-\theta F \Delta \Psi / RT}} - \frac{[\text{fADP}]_x}{[\text{fADP}]_x + [\text{fATP}]_x e^{+(1-\theta) F \Delta \Psi / RT}} \right) \left( \frac{1}{1 + k_{\text{m,ADP}} / [\text{fADP}]_i} \right) \quad (\text{A10})$$

where  $\theta$  is an empirical parameter with value set to 0.35. The phosphate-hydrogen cotransporter flux

$$J_{\text{PiHt}} = X_{\text{PiHt}} \left( \frac{[\text{H}_2\text{PO}_4^-]_i [\text{H}^+]_c - [\text{H}_2\text{PO}_4^-]_x [\text{H}^+]_i}{[\text{H}_2\text{PO}_4^-]_i + k_{\text{PiHt}}} \right) \quad (\text{A11})$$

where

$$[\text{H}_2\text{PO}_4^-]_i = [\text{H}^+]_i [\text{P}_i] / ([\text{H}^+]_i + k_{\text{dH}}) \text{ and} \quad (\text{A12})$$

$$[\text{H}_2\text{PO}_4^-]_x = [\text{H}^+]_x [\text{P}_i] / ([\text{H}^+]_x + k_{\text{dH}})$$

Mitochondrial adenylate kinase flux

$$J_{\text{AKi}} = X_{\text{AK}} (K_{\text{AK}} [\text{ADP}]_i [\text{ADP}]_i - [\text{AMP}]_i [\text{ATP}]_i) \quad (\text{A13})$$

Proton leak flux

$$J_{\text{Hle}} = X_{\text{Hle}} \Delta \Psi \left( \frac{[\text{H}^+]_c e^{+F \Delta \Psi / RT} - [\text{H}^+]_x}{e^{+F \Delta \Psi / RT} - 1} \right) \quad (\text{A14})$$

Potassium-hydrogen ion exchange

$$J_{\text{KH}} = X_{\text{KH}} ([\text{K}^+]_c [\text{H}^+]_x - [\text{K}^+]_x [\text{H}^+]_c) \quad (\text{A15})$$

#### Mathematical expressions for cytoplasmic reaction fluxes

Four biochemical processes are modeled in the cytoplasm—the adenylate kinase reaction, the creatine kinase reaction, ATP hydrolysis, and binding of magnesium ions to ADP and ATP.

The binding of magnesium to ATP and ADP in the cytoplasm takes the same form as the binding fluxes in the mitochondria

$$J_{\text{MgATPc}} = X_{\text{MgA}} ([\text{fATP}]_c [\text{Mg}^{2+}]_c - K_{\text{Mg-ATP}} [\text{mATP}]_c) \quad (\text{A16})$$

$$J_{\text{MgADPc}} = X_{\text{MgA}} ([\text{fADP}]_c [\text{Mg}^{2+}]_c - K_{\text{Mg-ADP}} [\text{mADP}]_c)$$

where  $[\text{fATP}]_c$  and  $[\text{fADP}]_c$  denote magnesium unbound ATP and ADP in the cytoplasm. Similarly, the cytoplasmic adenylate kinase is analogous to the mitochondrial reaction

$$J_{\text{AKc}} = X_{\text{AK}} (K_{\text{AK}} [\text{ADP}]_c [\text{ADP}]_c - [\text{AMP}]_c [\text{ATP}]_c) \quad (\text{A17})$$

In Eq. A18,  $K_{\text{AK}}$  is the equilibrium constant for the reaction  $2\text{ADP} \rightleftharpoons \text{ATP} + \text{AMP}$ , and  $X_{\text{AK}}$  is the enzyme activity, which is set to a large enough value so that the reaction is effectively maintained in equilibrium.

The creatine kinase flux is modeled using the expression

$$J_{\text{CKc}} = X_{\text{CK}} (K_{\text{CK}} [\text{ADP}]_c [\text{CrP}]_c [\text{H}^+]_c - [\text{ATP}]_c [\text{Cr}]_c) \quad (\text{A18})$$

where the activity  $X_{\text{CK}}$  is set to a large enough value so that the equilibrium  $K_{\text{CK}} = ([\text{ATP}]_c [\text{Cr}]_c / [\text{ADP}]_c [\text{CrP}]_c [\text{H}^+]_c)_{\text{eq}}$  is maintained during simulations. The value of the apparent equilibrium constant assumed here (see Table 2) is calculated to account for the intracellular ionic strength and magnesium ion concentration (25).

The flux  $J_{\text{AIC}}$  is defined as the flux through the reaction  $\text{ATP} \rightarrow \text{ADP} + \text{P}_i$ . Mathematical models for the ATP consumption flux are considered in the Results section.

#### Modification of the Model for Patients with Complex I Deficiency

Equation A1 assumes that 4 protons are pumped from the matrix to the intermembrane space for each pair of electrons transferred via the reaction at complex I. For patients with complex I deficiency, it is assumed that no protons are pumped at complex I, and the equations for  $[\text{H}^+]_x$  and  $\Delta \Psi$  are modified as follows

$$d[\text{H}^+]_x / dt = \beta^{-1} [\text{H}^+]_x (+J_{\text{DH}} - J_{\text{Cl}} - 2J_{\text{C3}} - 4J_{\text{C4}} + (n_A - 1)J_{\text{F1}} + 2J_{\text{PiHt}} - J_{\text{KH}} + J_{\text{Hle}}) / W_x \quad (\text{A19})$$

$$d\Delta \Psi / dt = (2J_{\text{C3}} + 4J_{\text{C4}} - n_A J_{\text{F1}} - J_{\text{ANT}} - J_{\text{Hle}}) / C_{\text{IM}}$$

#### ACKNOWLEDGMENTS

We thank Dr. H. R. Scholte for sharing oxygen polarographic data of isolated mitochondria of the complex I-deficient patients.

#### GRANTS

This work was supported by the National Institutes of Health Grants HL-072011 and EB-005825.

#### REFERENCES

1. **Alberty RA.** *Thermodynamics of Biochemical Reactions.* Hoboken, NJ: Wiley, 2003.
2. **Bakker HD, Scholte HR, Jeneson JA.** Vitamin E in a mitochondrial myopathy with proliferating mitochondria. *Lancet* 342: 175–176, 1993.
3. **Bakker HD, Scholte HR, Van den Bogert C, Ruitenbeek W, Jeneson JA, Wanders RJ, Abeling NG, Dorland B, Sengers RC, Van Gennip AH.** Deficiency of the adenine nucleotide translocator in muscle of a patient with myopathy and lactic acidosis: a new mitochondrial defect. *Pediatr Res* 33: 412–417, 1993.
4. **Beard DA.** A biophysical model of the mitochondrial respiratory system and oxidative phosphorylation. *PLoS Comput Biol* 1: e36, 2005.
5. **Beard DA.** Integrated computational modeling of oxygen transport and cellular energetics explains observations on in vivo cardiac oxygen consumption and energy metabolites. *PLoS Comput Biol.* In press.
6. **Blei ML, Conley KE, Kushmerick MJ.** Separate measures of ATP utilization and recovery in human skeletal muscle. *J Physiol* 465: 203–222, 1993.
7. **Chance B, Eleff S, Bank W, Leigh JS Jr, Warnell R.** 31P NMR studies of control of mitochondrial function in phosphofructokinase-deficient human skeletal muscle. *Proc Natl Acad Sci USA* 79: 7714–7718, 1982.
8. **Chance B, Leigh JS Jr, Clark BJ, Maris J, Kent J, Nioka S, Smith D.** Control of oxidative metabolism and oxygen delivery in human skeletal muscle: a steady-state analysis of the work/energy cost transfer function. *Proc Natl Acad Sci USA* 82: 8384–8388, 1985.
9. **Cortassa S, Aon MA, Marban E, Winslow RL, O'Rourke B.** An integrated model of cardiac mitochondrial energy metabolism and calcium dynamics. *Biophys J* 84: 2734–2755, 2003.
10. **Gentet LJ, Stuart GJ, Clements JD.** Direct measurement of specific membrane capacitance in neurons. *Biophys J* 79: 314–320, 2000.
11. **Jeneson JA.** *In vivo* <sup>31</sup>P NMR Studies of Cellular Bioenergetics in Healthy and Diseased Human Skeletal Muscle (PhD thesis). Utrecht, The Netherlands: Utrecht University, 1992.
12. **Jeneson JA, van Dobbenburgh JO, van Echteld CJ, Lekkerkerk C, Janssen WJ, Dorland L, Berger R, Brown TR.** Experimental design of <sup>31</sup>P MRS assessment of human forearm muscle function: restrictions imposed by functional anatomy. *Magn Reson Med* 30: 634–640, 1993.
13. **Jeneson JA, Westerhoff HV, Brown TR, van Echteld CJ, Berger R.** Quasi-linear relationship between Gibbs free energy of ATP hydrolysis and power output in human forearm muscle. *Am J Physiol Cell Physiol* 268: C1474–C1484, 1995.
14. **Jeneson JA, Wiseman RW, Westerhoff HV, Kushmerick MJ.** The signal transduction function for oxidative phosphorylation is at least second order in ADP. *J Biol Chem* 271: 27995–27998, 1996.
15. **Kushmerick MJ.** Energy balance in muscle activity: simulations of ATPase coupled to oxidative phosphorylation and to creatine kinase. *Comp Biochem Physiol B Biochem Mol Biol* 120: 109–123, 1998.
16. **Kushmerick MJ, Meyer RA, Brown TR.** Regulation of oxygen consumption in fast- and slow-twitch muscle. *Am J Physiol Cell Physiol* 263: C598–C606, 1992.
17. **Lee AC, Zizi M, Colombini M.**  $\beta$ -NADH decreases the permeability of the mitochondrial outer membrane to ADP by a factor of 6. *J Biol Chem* 269: 30974–30980, 1994.
18. **Meyer RA.** A linear model of muscle respiration explains monoexponential phosphocreatine changes. *Am J Physiol Cell Physiol* 254: C548–C553, 1988.
19. **Mizuno M, Horn A, Secher NH, Quistorff B.** Exercise-induced 31P-NMR metabolic response of human wrist flexor muscles during partial

- neuromuscular blockade. *Am J Physiol Regul Integr Comp Physiol* 267: R408–R414, 1994.
20. **Munoz DR, de Almeida M, Lopes EA, Iwamura ES.** Potential definition of the time of death from autolytic myocardial cells: a morphometric study. *Forensic Sci Int* 104: 81–89, 1999.
  21. **Pybus J, Tregear RT.** The relationship of adenosine triphosphatase activity to tension and power output of insect flight muscle. *J Physiol* 247: 71–89, 1975.
  22. **Roef MJ, Reijngoud DJ, Jeneson JA, Berger R, de Meer K.** Resting oxygen consumption and in vivo ADP are increased in myopathy due to complex I deficiency. *Neurology* 58: 1088–1093, 2002.
  23. **Saks VA, Kongas O, Vendelin M, Kay L.** Role of the creatine/phospho-creatine system in the regulation of mitochondrial respiration. *Acta Physiol Scand* 168: 635–641, 2000.
  24. **Tomashek JJ, Brusilow WS.** Stoichiometry of energy coupling by proton-translocating ATPases: a history of variability. *J Bioenerg Biomembr* 32: 493–500, 2000.
  25. **Veech RL, Lawson JW, Cornell NW, Krebs HA.** Cytosolic phosphorylation potential. *J Biol Chem* 254: 6538–6547, 1979.
  26. **Vendelin M, Kongas O, Saks V.** Regulation of mitochondrial respiration in heart cells analyzed by reaction-diffusion model of energy transfer. *Am J Physiol Cell Physiol* 278: C747–C764, 2000.
  27. **Vendelin M, Lemba M, Saks VA.** Analysis of functional coupling: mitochondrial creatine kinase and adenine nucleotide translocase. *Biophys J* 87: 696–713, 2004.
  28. **Vicini P, Kushmerick MJ.** Cellular energetics analysis by a mathematical model of energy balance: estimation of parameters in human skeletal muscle. *Am J Physiol Cell Physiol* 279: C213–C224, 2000.
  29. **Vinnakota KC, Bassingthwaight JB.** Myocardial density and composition: a basis for calculating intracellular metabolite concentrations. *Am J Physiol Heart Circ Physiol* 286: H1742–H1749, 2004.
  30. **Vogt M, Puntschart A, Geiser J, Zuleger C, Billeter R, Hoppeler H.** Molecular adaptations in human skeletal muscle to endurance training under simulated hypoxic conditions. *J Appl Physiol* 91: 173–182, 2001.
  31. **Westerhoff HV, van Echteld CJ, Jeneson JA.** On the expected relationship between Gibbs energy of ATP hydrolysis and muscle performance. *Biophys Chem* 54: 137–142, 1995.
  32. **Zhang J, Ugurbil K, From AH, Bache RJ.** Myocardial oxygenation and high-energy phosphate levels during graded coronary hypoperfusion. *Am J Physiol Heart Circ Physiol* 280: H318–H326, 2001.

